Tissue and Cell 99 (2026) 103256

Contents lists available at ScienceDirect

Tissue and Cell

journal homepage: www.elsevier.com/locate/tice

In vitro osteogenic potential of magnesium alloy without and with calcium phosphate coating

Mariana de Oliveira Viana Veras [a,1], Fátima Regina Nunes de Sousa [b,2], Conceição Silva Martins [c,3], Gildênio Estevam Freire [a,4], Ana Beatriz Graça Duarte [a,5], Thâmara Manoela Marinho Bezerra [c,6], Yves Ramos Costa Beviláqua [c,7], Stephany Ellen de Castro [c,8], Matheus Brandão dos Santos Lopes [c,9], Rosemayre Souza Freire [d,10], Pierre Basílio Almeida Fechine [e,11], Abrahão Cavalcante Gomes de Souza Carvalho [f,12], Paula Goes [g,13], Mirna Marques Bezerra [a,h,*,14], Renata Ferreira Carvalho Leitão [a,c,*,15]

[a] Postgraduate Program in Morphofunctional Sciences, Department of Morphology, School of Medicine, Federal University of Ceará, Fortaleza, Ceará, Brazil
[b] Department of Morphology, Medical School, Federal University of Piaui, Picos, Piauí, Brazil
[c] Department of Morphology, School of Medicine, Federal University of Ceará, Fortaleza, Ceará, Brazil
[d] Analytical Center, Federal University of Ceará, Fortaleza, Ceará, Brazil
[e] Department of Analytical and Physical Chemistry, Federal University of Ceará, Fortaleza, Ceará, Brazil
[f] Department of Clinical Dentistry, Faculty of Pharmacy, Dentistry and Nursing, Federal University of Ceará, Fortaleza, Ceará, Brazil
[g] Department of Pathology and Legal Medicine, Medical School, Federal University of Ceará Fortaleza, Ceará, Brazil
[h] Postgraduate Program in Health Sciences, Medical School, Federal University of Ceará, Sobral, Ceará, Brazil

ARTICLE INFO

Keywords:
Osteoblasts
Magnesium
Phosphate
Biomaterials test
Biocompatibility test

ABSTRACT

Magnesium-based biomaterials have emerged as promising candidates for bone regeneration due to their biodegradability and favorable mechanical properties. This study investigated the effects of Magnesium alloys without (Mg1) and with (Mg2) calcium phosphate coating on osteoblast viability and activation. The physical structure of the alloys was analyzed by surface characterization, mechanical testing, and biodegradation assays. Biological performance was evaluated through MTT and MTS assays for cell viability and proliferation, quantification of alkaline phosphatase activity at 24 h, 7, and 15 days, and mineralization by Von Kossa staining, after

* Correspondence to: Departamento de Morfologia, Faculdade de Medicina, Universidade Federal do Ceará, Rua Delmiro Farias 1331, Rodolfo Teófilo, Fortaleza, Ceará 60430-170, Brazil.

E-mail addresses: vianaverasodontologia@gmail.com (M.O.V. Veras), fatimaregina.cd@ufpi.edu.br (F.R.N. Sousa), josycristophe@ufc.br (C.S. Martins), estevamgildenio@gmail.com (G.E. Freire), beatrizgduarte@ufc.br (A.B.G. Duarte), yvesbevilaqua@hotmail.com (Y.R.C. Beviláqua), castrostee@gmail.com (S.E. de Castro), matheusnegrao972@gmail.com (M.B.S. Lopes), rosefreire@fisica.ufc.br (R.S. Freire), fechine@ufc.br (P.B.A. Fechine), abrahao@ufc.br (A.C.G. Souza Carvalho), paulagoes@ufc.br (P. Goes), mirna@ufc.br (M.M. Bezerra), renata.carvalho@ufc.br (R.F.C. Leitão).

[1] ORCID: 0000–0003-0778–6088
[2] ORCID: 0000–0002-9875–3718
[3] ORCID: 0000–0001-8710–1856
[4] ORCID: 0000–0001-8682–9183
[5] ORCID: 0000–0002-0403–4254
[6] ORCID: (0000–0001-5502–8949)
[7] ORCID: 0000–0003-1534–1265
[8] ORCID: 0000–0002-5866–338X
[9] ORCID: (0000–0002-4248–351X)
[10] ORCID: 0000–0003-4430–5298
[11] ORCID: 0000–0002-7822–2354
[12] ORCID: 0000–0002-0581–2468
[13] ORCID: 0000–0002-9704–2412
[14] ORCID: 0000–0003-2146–4456
[15] ORCID: 0000–0003-0202–771X

https://doi.org/10.1016/j.tice.2025.103256
Received 2 June 2025; Received in revised form 13 October 2025; Accepted 28 November 2025
Available online 29 November 2025

21 days. Cell morphology and apoptosis were assessed using fluorescence microscopy and immunostaining for caspase 3 and 9, while protein expression of BMP-2, OPG, and RANK-L was also investigated by immunostaining. The results demonstrated a significant increase in viable cells in both Mg1 and Mg2 groups after 24 and 48 h. Enhanced mineralization and a significant increase in alkaline phosphatase activity were observed in the Mg2 group. Both Mg1 and Mg2 groups exhibited a similar reduction in caspases 3 and 9 expression, indicating cell survival despite morphological changes. Furthermore, osteoblasts cultured on both alloys showed greater expression of BMP-2 and OPG, compared to the DMEM group. Taken together, these findings highlight the potential of calcium phosphate-coated magnesium alloy as a novel approach for bone restoration in the future.

1. Introduction

With the progressive increase in life expectancy, the prevalence of age-related disorders such as osteopenia and osteoporosis has also increased. These metabolic conditions are characterized by a gradual reduction in bone mineral density and a consequent increase in the risk of fractures and bone defects (Pereira et al., 2011). One of the significant challenges in tissue engineering and regenerative medicine is the treatment of such defects, which are marked by extensive bone loss and an impaired ability of the tissue to regenerate spontaneously (Black et al., 2015). In this context, the development of biomaterials capable of supporting the repair of damaged tissues and restoring their physiological functions promptly become a central focus of global research efforts (Farag, 2023).

Among the materials proposed for bone repair, magnesium and calcium phosphates stand out as particularly promising due to their favorable interactions with living tissues. Magnesium alloys, in particular, exhibit several advantageous properties: they are fully biodegradable, have mechanical characteristics similar to bone, do not trigger inflammatory or systemic responses, are osteoconductive, and actively stimulate bone formation (Cheng et al., 2016). In addition, their biodegradability eliminates the need for a second surgical procedure to remove the scaffold when otherwise required. Taken together, these features suggest that magnesium (Mg) holds significant potential as a load biomaterial (Sezer et al., 2018).

The degradation rate of magnesium alloys must be carefully controlled to enable their application as orthopedic devices, including screws and fixation plates, in bone reconstruction surgeries (Kieke et al., 2016). Rapid and unpredictable degradation compromises the mechanical integrity of the implant, thereby limiting its clinical applicability (Wong et al., 2013); therefore, it is crucial to control the degradation rate of Mg under physiological conditions. Calcium phosphate (CaP) is a well-established osteoconductive material that, in vivo, exhibits a considerably slower degradation rate compared to magnesium (Iskandaret al., 2015). For this reason, CaP-based coatings are widely employed to regulate the corrosion behavior of Mg alloys. Acting as protective barriers, these coatings reduce the penetration of water and aggressive ions into the Mg substrate, thereby decreasing the degradation rate and mitigating the alkalinization of the surrounding medium (Gonzalez et al., 2018). In addition, phosphate ions (PO^{3-}) assist in the precipitation of Mg phosphates, which decrease the formation of corrosion spots (Xin et al., 2008). Given that calcium phosphate ($Ca_3(PO_4)^2$) constitutes the main mineral phase of bone, it represents an ideal covering material, not only providing a protective layer but also enhancing bone integration and promoting osteoblast response (Song et al., 2010).

In this context, the present work evaluated standard parameters, including mechanical properties and biodegradation rates, to evaluate the performance and stability of Mg alloys, uncoated (Mg1) and CaP-coated (Mg2). In addition, their osteogenic potential (cell viability, proliferation, activation, and overall biocompatibility) was investigated using murine osteoblasts.

2. Materials and methods

2.1. Biomaterial preparation and coating protocol

Calcium phosphate coating (CaP) was obtained through a precipitation method conducted in an aqueous medium. The technique involves reactions between calcium and phosphate precursors, under regulated temperature and pH conditions. A precursor solution was prepared by mixing 50 mL of calcium hydroxide (0.5 mM), 50 mL of orthophosphoric acid (0.3 mM), and 50 mL of lactic acid (1.6 mM) (Wang, 2011).

High-purity magnesium (99.99 %) was used for the coating production. Samples were cleaned by ultrasonic treatment in mild detergent, acetone, and distilled water (10 min each). The cleaned Mg samples were then subjected to one-step hydrothermal treatment by immersion in the precursor solution at 80°C (Xie et al., 2002).

2.2. Mechanical test

The mechanical properties of Magnesium alloys (strain-stress curve) were analyzed through uniaxial tensile tests, using a Universal Testing Machine Instron 3345 (Instron Corporation, Canton, MA, USA), with a displacement speed of 0,5 $mm.min^{-1}$, a 500-load cell, and a distance between the grips of 10 cm. Specimens were cut into a rectangular shape (10 cm x 4 mm), and 15 samples for each test were evaluated. The testing procedure and specimen used were in accordance with the ASTM E517–18 standard for metallic materials (Cherkaev and Bonifasi-Lista, 2011).

2.3. Structural and morphological characterization

The structural characterization of the coated samples was performed by X-ray diffraction (XRD) using an XPERT Pro MPD diffractometer (PANanalytical) with CoKα radiation (40 kV, 40 mA) in the 2θ range of 20–60°. The surface morphology was analyzed by scanning electron microscopy (SEM) using a Quanta 450FEG (FEI-Company, Hillsboro, OR, USA).

2.4. Biodegradation rates

The Magnesium alloys were sterilized in a 12 L autoclave (Cristófoli, Paraná, Brazil), cut into 1 cm× 4 mm pieces, and immersed in a 12-well plate with 5 mL of DMEM per well with a minimum volume of solution for the sample area according to American Society of Testing Materials (ASTM) G31–72 (9). The plate was placed in an incubator to simulate the physiological conditions suffered by the biomaterial, and the pH values of the medium were measured with a pH meter (Kasvi, São José dos Pinhais, PR, Brazil) at three different periods: 24 h, 7 days, and 15 days after immersion (Cui et al., 2008).The samples were divided into 3 groups; each group being allocated in 4 wells: control- DMEM; Mg1 – Magnesium alloys immersed in DMEM, and Mg2 – Calcium Phosphate-coated Magnesium alloys immersed in DMEM. Photographs of the biomaterial were also taken after the three different periods. The images were standardized at the same distance to allow the comparison of the degradation area. For this, the images were measured using the ImageJ 1.51 j8 software. The software calculates the biomaterial

degradation area of each group. This area was calculated initially in pixels and then converted into mm (Saleh et al., 2016).

2.5. In vitro tests

Murine osteoblasts (OFCOL II), obtained from the cell bank of the Federal University of Rio de Janeiro, were maintained in DMEM culture medium (Dulbencoo's Modified Essential Medium) supplemented with 10 % fetal bovine serum (FBS) and 1 % antibiotics (100 U/mL penicillin and 100 µg/mL streptomycin), incubated in a 37°C incubator with 5 % CO_2 (Sanyo, Osaka, Japan) (Hiromoto et al., 2017).

To perform the tests, the samples were divided into 3 groups, as follows: Control – OFCOLL II cells plated directly into culture plate wells with supplemented DMEM culture medium; Mg1 – OFCOLL II cells cultivated on Magnesium alloys in supplemented DMEM culture medium; Mg2 – OFCOLL cells cultivated on calcium phosphate-coated Magnesium alloys in supplemented DMEM culture medium.

2.6. Cell viability, proliferation, and metabolic activity by MTT and MTS

For both assays, OFCOLL II cells were cultured in a 96-well plate containing 100 µl DMEM and 3 × 104 cells per well at 24 and 48 h. For the MTT, after the mentioned periods, 20 µl per well of MTT, diluted in PBS to a concentration of 5 mg/mL, was added. MTT (3-(4,5 4,5-dimethylthiazol-2-yl)-2,5-diphenyl tetrazolium bromide (Sigma, St. Louis, MO, USA) was incubated for 3 h. After this time, the entire contents of the wells were removed, and 100 µl DMSO was added to each well. The solution was aspirated and transferred to a new 96-well plate without the biomaterial, and absorbance readings were taken on a spectrophotometer (Biotek, Winooski, VT, USA) at a wavelength of 590 nm (Park et al., 2013).

For the MTS, after incubation, cell proliferation was assessed using 3-(4,5-dimethylthiazol-2-yl)-5-(3-carboxymethoxyphenyl)-2-(4-sulfophenyl)-2H tetrazolium assay (CellTiter 96 Aqueous, Promega, Madison, WI, USA). Formazan accumulation was quantified by the absorbance at 490 nm using a spectrophotometer (Biotek, Winooski, VT, USA) (Moss, 1982).

2.7. Alkaline phosphatase activity

OFCOLL II cells were cultured in a 24-well plate containing 400 µl DMEM and 7 × 10^3 cells per well, then, samples of medium supernatants were collected after 24 h, 48 h and 7 days. After collection, alkaline phosphatase levels (APL) were measured using a specific kit, whose methodology followed the manufacturer's laboratory instructions (LABTEST®, Lagoa Santa, MG, Brazil) (Arganda-Carreras et al., 2017).

2.8. Mineral nodules formation (Von Kossa mineralization assay)

OFCOLL II cells were incubated in a 12-well culture plate at a concentration of 3 × 104 cells per well, and the culture medium was changed every 48 h. The mineralization analysis was performed within 21 days. At the end, the culture medium was removed, each well was washed with PBS, and the cells were fixed with 100 % ethanol (1 mL/well) for 30 min. The cells were then rehydrated in decreasing concentrations of ethanol (100–50 % for 5 min in each solution) and washed in distilled water twice. Then 1 mL of 5 % silver nitrate solution (AgNO3) was placed in each well, and the cells were exposed to UV light for 1 h. Analyses were made from photographs using the inverted microscope at 40x magnification (Köhler et al., 2002).

For the quantitative morphometric analysis, five random Von Kossa slide sections were electronically digitized into an RGB image, which was later analyzed using Image-J software (NIH, Bethesda, MD, USA).

2.9. Cell morphology by immunofluorescence

OFCOLL II cells were cultured at a concentration of 5 × 10^4 cells per well in a 4-well cell culture plate (35 mm×10 mm). After 24 h, the medium was removed and the cells, together with the Magnesium alloys, were fixed with 500 µL of 4 % paraformaldehyde (PFA) per well for 30 min. Then, 500 µL of blocking solution was used for 1 h, followed by incubation with phalloidin (1:400; Santa Cruz, Dallas, TX, USA), for cytoskeleton staining, and maintained for 2 h. After this period, 100 µL of primary Alexa Fluor 594 antigen (Invitrogen, Waltham, MA, USA) was diluted in the washing solution for 30 min. Then, the cell nucleus was stained with DAPI (1:2000) diluted in 1x PBS for 5 min. All steps were interspersed with successive washes with the wash buffer. The preparations were observed using a confocal microscope (LM710-Confocal-Zeiss, Oberkochen, Germany) with selective filters for each fluorophore, and images were captured with an integrated camera and image processor (Iskandar et al., 2015). For a better analysis of the images, two subgroups were created: (1) OFCOLL II cells adhered to the biomaterial, and (2) OFCOLL II cells adhered to the culture plate.

2.10. Osteoblast apoptosis by immunofluorescence

Osteoblasts were cultured at a concentration of 5 × 104 cells per well in a 4-well cell culture plate (35 mm×10 mm). After 24 h, the medium was removed and the cells, together with the Magnesium alloys, were fixed with 500 µL of 4 % paraformaldehyde (PFA) per well for 30 min. Then, 500 µL of blocking solution was used for 1 h, followed by incubation with diluted primary antibodies for Caspase 3 (1:100) and Caspase 9 (1:100) (Santa Cruz, Dallas, TX, USA), which were maintained for 4 h. After that period, 100 µL of the secondary antibody Alexa Fluor 594 (Invitrogen, Waltham, MA, USA) diluted in the washing solution was added for 30 min. Then, the cell nucleus was stained with DAPI (1: 2000) diluted in 1x PBS for 5 min. All steps were interspersed with successive washes with wash buffer. The preparations were observed in a confocal microscope (LM710- Confocal-Zeiss, Oberkochen, Germany), using selective filters for each fluorophore; the images were captured with an integrated camera and image processor (Nogueira-Júnior et al., 2024).

2.11. BMP-2, OPG, and RANKL production by osteoblasts

OFCOLL II cells were cultured at a concentration of 5 × 104 cells per well in a cell culture dish (35 mm×10 mm). After 24 h, the medium was removed and the cells, together with the Magnesium alloys, were fixed with 500 µL of 4 % paraformaldehyde (PFA) per well for 30 min. Then, 500 µL of blocking solution was used for 1 h, followed by incubation with the diluted primary antibodies for RANK-L (1:100), OPG (1:100), and BMP-2 (1:200) (Santa Cruz, Dallas, TX, USA) for 4 h. After this period, 100 µL of secondary Alexa Fluor 594 anti-rabbit antibody (Invitrogen, Waltham, MA, USA) diluted in washing solution was added and incubated for 30 min. Then, the cell nucleus was stained with DAPI (1: 2000) diluted in 1x PBS for 5 min. All steps were interspersed with successive washes. The preparations were observed using a confocal microscope (LM710-Confocal-Zeiss, Oberkochen, Germany), equipped with selective filters for each fluorophore. The images were captured with an integrated camera and image processor. The number of immunostained cells per field was obtained using the Image J (NIH, Bethesda, MD, USA) program to quantify the number of positive cells labeled with BMP-2, OPG, and RANK-L. Ten fields per slide were photographed with a total of 4 slides per group (Jilka et al., 2013).

A quantitative analysis of these images was conducted using a scoring system with modifications (Fedchenko and Reifenrath, 2014). For this, the cells were categorized according to the intensity of the nucleus staining (stained with DAPI) and the cytoskeleton (stained with the antibodies: RANK-L, OPG, and BMP-2). The cells that show diffuse and low intensity labeling were called weak (+), and as the marking became more evident and more intense, they were called moderate (++)

and strong (+++) (Cowin, 2001). Three evaluators analyzed the images in a blind study, and the scores were expressed as median, minimum, and maximum values.

2.12. Statistical analysis

Shapiro-Wilk was used to assess normality. One or two-way analysis of variance (ANOVA) followed by the Bonferroni test was used to compare the averages obtained. Values were expressed as Mean ± Mean Standard Error. Non-parametric data were analyzed by the Kruskal-Wallis test followed by Dunn's multiple comparisons test. The level of significance was considered at $P < 0.05$. The analysis was performed using the GraphPad Prism 7 program (GraphPad Prism Software, La Jolla, CA, USA).

3. Results

3.1. Analysis of chemical and physical characteristics of Magnesium alloys without and with calcium phosphate coating

In the traction test, Magnesium alloys exhibit tensile strength of 147 MPa. XRD analysis of the coated samples revealed characteristic peaks of crystalline calcium phosphate dihydrate (brushite, DCPD; JCPDS No. 072–0713) and minor peaks of magnesium (JCPDS No. 004–0770), confirming the successful deposition of the CaP coating on the substrate (Fig. 1A). Fig. 1B presents the SEM micrograph of the coated Mg surface, revealing a rough and irregular morphology with granular CaP deposits uniformly distributed across the metallic substrate. The coating appeared compact and continuous, exhibiting microporosities and clusters of crystalline structures consistent with CaP deposition.

Quantitative analysis of surface degradation (Fig. 1C) revealed smaller areas for Mg1 compared with Mg2 at all time points: day 1 (47,000 ± 2000 *vs.* 54,000 ± 3000 mm^2), day 7 (39,000 ± 2500 *vs.* 47,000 ± 4000 mm^2), and day 15 (28,000 ± 3000 *vs.* 42,000 ± 5000 mm^2). Representative images (Fig. 1D) corroborated these findings, showing a more pronounced size reduction for Mg1 after 15 days.

Fig. 1E depicts the pH variations in the culture medium over the 15-day period. At day 1, DMEM, Mg1, and Mg2 reached 7.9, 8.2, and 8.4, respectively. By day 7, the values increased to 8.4 (DMEM), 8.5 (Mg1), and 9.1 (Mg2). At day 15, pH values were 8.9 for DMEM, 9.3 for Mg1, and 9.8 for Mg2.

3.2. Evaluation of Magnesium alloys without and with calcium phosphate coating and its influence on viability, proliferation, and activation of murine osteoblasts

MTT assays (Fig. 2A–B) showed that Mg1 and Mg2 significantly increased cell viability compared with DMEM at both 24 h (0.43 ± 0.06 and 0.38 ± 0.04 vs. 0.18 ± 0.05) and 48 h (0.18 ± 0.02 and 0.19 ± 0.02 vs. 0.12 ± 0.01; $P < 0.05$), indicating absence of cytotoxicity. Proliferation (Fig. 2C–D) also remained higher in Mg1 and Mg2 than in DMEM, with values of 138 ± 7 and 140 ± 4 at 24 h and 149 ± 5 and 151 ± 4 at 48 h, compared to 95 ± 5 and 95 ± 7 in DMEM ($P < 0.05$). No significant differences were detected between Mg1 and Mg2 at either time point.

The results of the alkaline phosphatase test are expressed in Fig. 3A. After 15 days, both Mg1 (23 ± 2) and Mg2 (27 ± 2) exhibited significantly ($P < 0.05$) higher alkaline phosphatase activity compared with the Control group (18 ± 1.5).

Fig. 3B and 3 C show mineralization nodules in osteoblast cultures incubated with Mg1 and Mg2 alloys, as revealed by Von Kossa staining. After 21 days, osteoblasts cultured on Mg alloys exhibited greater nodule formation compared with the DMEM group (Fig. 3C I). Notably, the Mg2 group displayed a higher number and larger size of nodules (21 ± 2.5) than both the control (10 ± 2) and Mg1 (15 ± 2.5) groups. Representative images (Fig. 3C II and 3 C III) further confirm the increased quantity and size of mineralization nodules in Mg-treated cultures.

Fig. 3D illustrates OFCOLL II cells adhered to the Magnesium alloys and OFCOLL II cells adhered to the culture plate (around the Magnesium alloy tapes). Cells directly on both Magnesium alloys presented undefined cytoskeleton morphology, while the cells adhered around the Magnesium alloys showed their normal spindle-shaped morphology.

Fig. 4 shows a qualitative immunofluorescence analysis of caspase-3 and caspase-9 expression in OFCOL II cells, demonstrating that the Mg1 and Mg2 groups, where the cells were grown directly on the biomaterial, showed lower expression of caspases 3 and 9, indicating that the cells remained viable despite lacking the typical spindle-shaped morphology.

Fig. 5 shows the expression of the BMP-2, OPG, and RANK-L proteins. OFCOL II cells cultivated on Mg1 and Mg2 alloys demonstrated a significant ($P < 0.05$) increase in BMP-2 expression relative to those cultured in DMEM [median (range): 1 (1–2) for DMEM; 2 (2–3) for Mg1; 2 (2–3) for Mg2; $P < 0.05$]. Similarly, OPG expression was increased in both the Mg1 and Mg2 groups [2 (1–3) for DMEM; 3 (2–3) for Mg1; 3 (2–3) for Mg2; $P < 0.05$]. Conversely, RANK-L expression exhibited no significant variation across the groups [2 (1–3) for DMEM; 2 (1–3) for Mg1; 2 (1–3) for Mg2] Fig. 5.

4. Discussion

This study assessed the physicochemical properties (mechanical test and biodegradation rates) and osteogenic potential of magnesium alloys (Mg), either uncoated (Mg1) or coated with calcium phosphate (Mg2), *in vitro,* using murine osteoblast (OFCOLL II). The presence of the coating significantly reduced the degradation rate. Neither alloy demonstrated cytotoxic effects; both promoted increased alkaline phosphatase activity, although the Mg2 group exhibited a greater number and size of mineralization nodules. Osteoblasts cultured directly on the biomaterial (Mg1 and Mg2) displayed reduced caspase 3 and 9 expression, consistent with preserved viability despite the absence of a typical fusiform shape. Moreover, both groups upregulated the expression of BMP-2 and OPG.

The Mg alloys evaluated in this study demonstrated a tensile strength of 147 MPa, which closely approximates the value reported for healthy human cortical bone (150 MPa). Biomaterials with tensile strength below that of bone are prone to premature fracture due to inadequate resistance to physiological stress. Conversely, material with excessively high strength may result in deleterious stress concentration at the bone-implant interface (Hart et al., 2017).

Magnesium is a biodegradable material characterized by favorable mechanical properties, such as strength and elasticity similar to those of bone, and by its potential to promote bone regeneration. Consequently, its application in alloy form has been extensively studied within the field of tissue engineering. However, rapid corrosion remains a significant limitation for clinical translation. This drawback can be mitigated through surface modification. In this study, calcium (Ca) and phosphate (P) were employed as coating elements, given their status as the predominant inorganic constituents of bone tissue.

Coating Mg alloys with calcium phosphate has been shown to decrease corrosion rates, thereby attenuating pH fluctuations, hydrogen evolution, and the release of electrochemical by-products that may interfere with bone tissue formation (Marco et al., 2017). This protective layer prevents direct exposure of Mg to the physiological environment, reducing the risk of toxic metal ions release due to corrosion or wear, which could otherwise elicit inflammatory or allergic responses (Cherkaev et al., 2011; Cui et al., 2008). Proper surface modification not only mitigates these adverse effects but also facilitates direct tissue integration (Oriňaková et al., 2020). Moreover, calcium phosphate coating has been consistently reported as an effective means of enhancing the

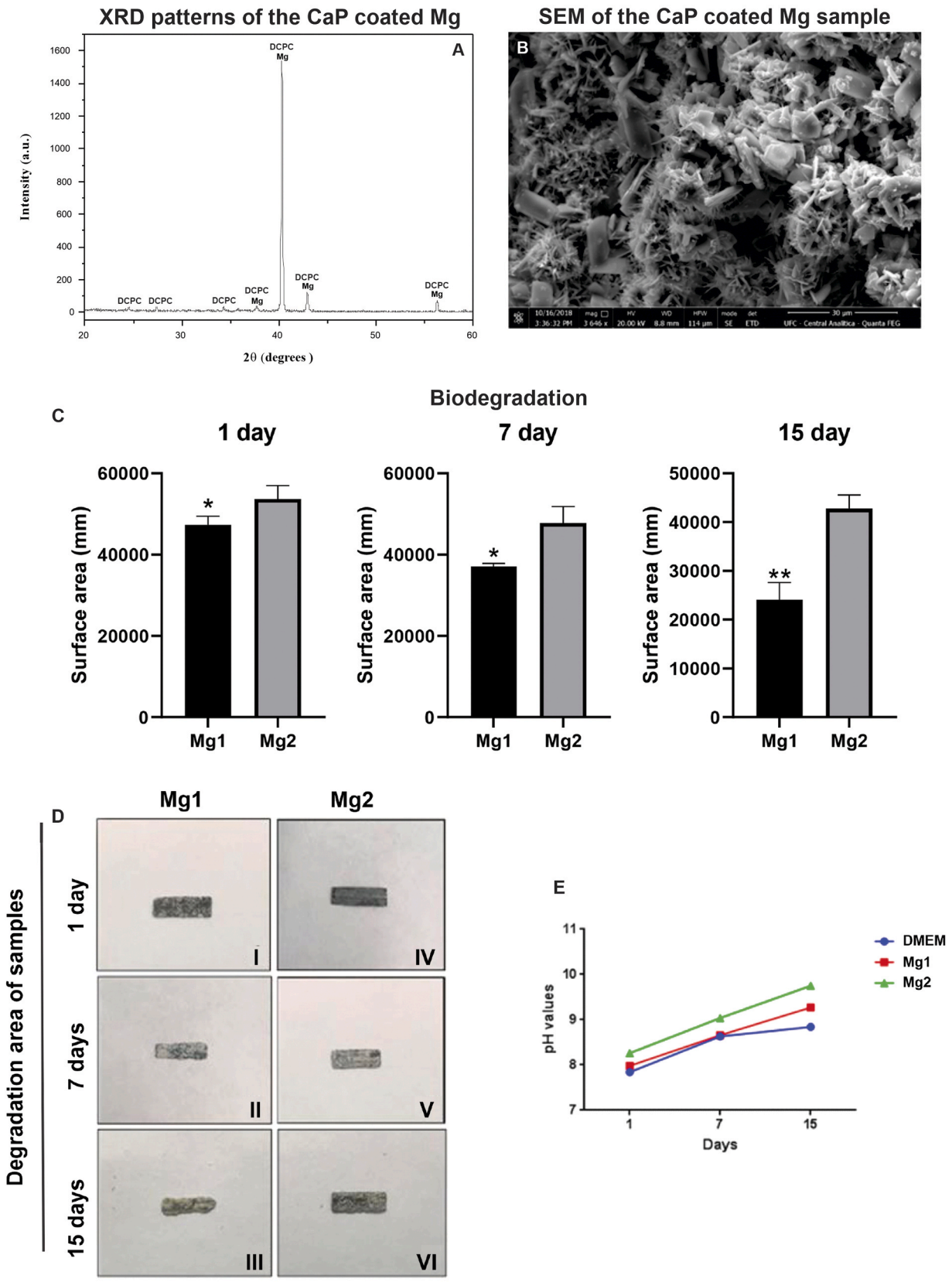

Fig. 1. A) X-ray diffraction (XRD) pattern of the magnesium alloy coated with calcium phosphate (Mg2). The diffractogram exhibits characteristic diffraction peaks confirming the presence of crystalline calcium phosphate phases on the Mg substrate, validating the successful deposition of the CaP coating. B) Scanning electron microscopy (SEM) image of the calcium phosphate coating on the Mg2 surface. The micrograph shows a homogeneous layer of plate-like crystals covering the substrate, confirming uniform surface deposition. C) Measurement (mm) of the degradation area of the samples from Magnesium alloy without (Mg1) and with (Mg2) Calcium Phosphate. D) Photographic images of samples from Mg1 and Mg2 after immersion test at three different time periods: 1, 7, and 15 days. E) pH values of the immersion medium of Mg1 and Mg2 in three different time periods: 1, 7, and 15 days.

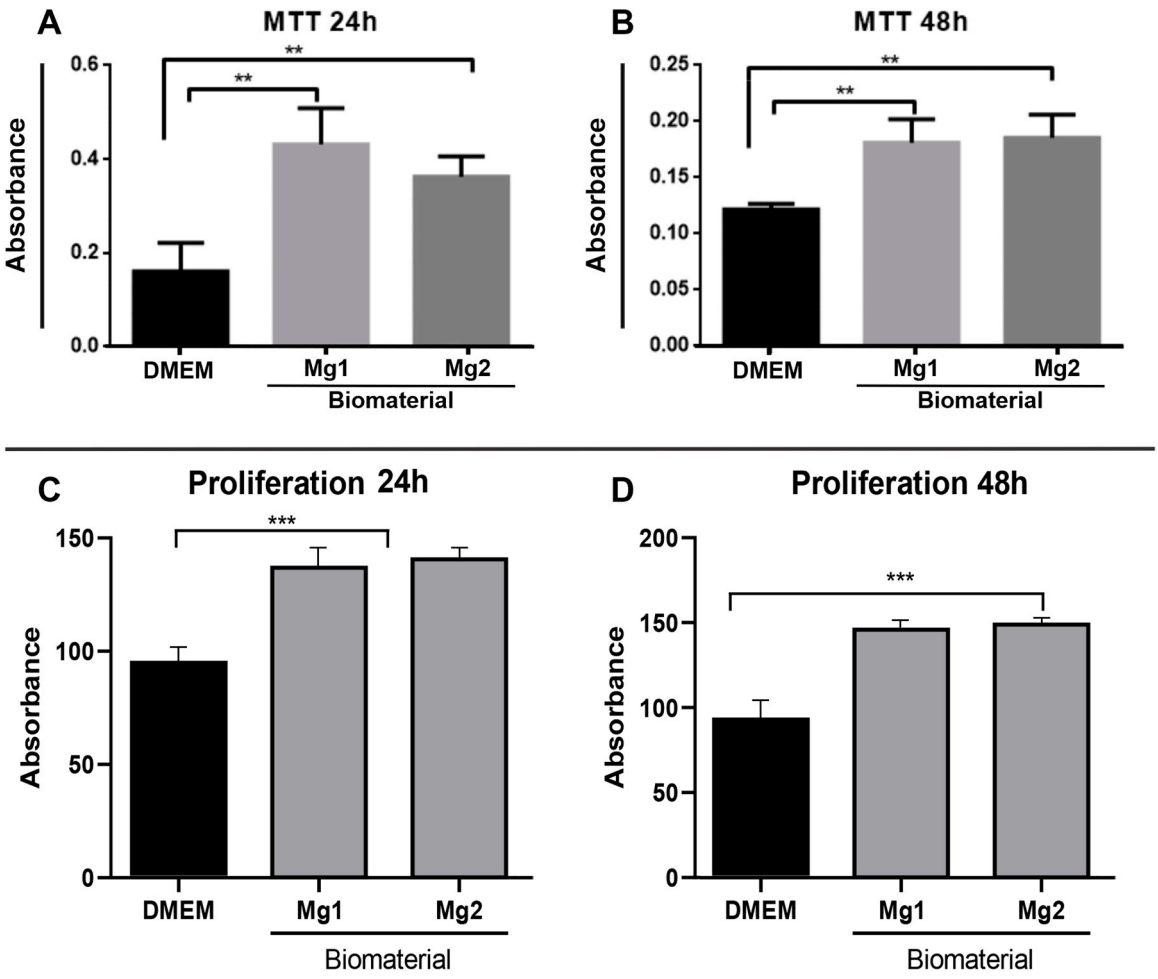

Fig. 2. Effect of Magnesium alloy without (Mg1) and with (Mg2) Calcium Phosphate coating on the viability (A and B) and proliferation (C and D) of murine osteoblasts (OFCOL II) after 24 h (A and C) and 48 h (B and D). DMEM group: cells cultured without biomaterial; Mg1 group: cells cultured with Mg1; Mg2 group: cultured with Mg2. *P $<$ 0.05 compared to the DMEM group.

bioactivity of the Mg alloys (Zhang et al., 2018). XRD examination in our study revealed the production of crystalline calcium phosphate phases on the alloy surface, so verifying the coating process and substantiating its role in enhancing stability and osteogenic response.

The application of calcium phosphate-coated biomaterials is advantageous in managing extensive bone defects, where long-term structural integrity is required, as they act as a temporary scaffold for bone regeneration. These biomaterials are gradually degraded and replaced by new bone, allowing for complete defect repair. A slower degradation profile is particularly relevant in pediatric reconstructive surgery, as it reduces the need for repeated interventions to replace the biomaterial during skeletal growth. Furthermore, Mg alloys present the added benefit of being fully synthetic, unlike collagen-based biomaterials commonly derived from bovine intestines (Pires et al., 2015). This characteristic is increasingly valuable in light of patient preferences to avoid the use of animal-derived products.

The biocompatibility of Mg alloys has been demonstrated across multiple cell lines, including pre-osteoblastic murine macrophages and fibroblasts (Klammert et al., 2009). The present findings corroborate these studies, as osteoblasts exposed to Mg alloys (Mg1 or Mg2) exhibited sustained viability, without evidence of cytotoxicity, at any evaluated time point. Moreover, the Mg2 group showed superior outcomes in terms of cell viability and proliferation, consistent with immersion assay data indicating enhanced corrosion resistance compared to the Mg1. These observations align with previous reports (Cheng et al., 2016; Wong et al., 2013) and may be attributed to the reduced evolution of H_2 gas and release of $Mg2+$ ions (Hiromoto and Yamazaki, 2017). In agreement, no alteration in the pH of the DMEM culture medium was detected, even after 15 days of exposure to Mg1 or Mg2 alloys.

In the present investigation, increased activity of alkaline phosphatase, an established marker of osteoblast function and differentiation (Benoit et al., 2008), was detected in both Mg1 and Mg2 groups. Osteoblast activity was further assessed through Von Kossa histological staining, which demonstrated the formation of mineralization nodules when compared to the DMEN group. Notably, the Mg2 group exhibited a greater number and larger size of nodules than both the control and Mg1 groups. These results indicate that osteoblasts cultured on Mg-based biomaterials remain metabolically active and capable of performing biological functions (Wennberg et al., 2000). Consistent with prior studies, our findings support the notion that increasing alkaline phosphatase activity is one of the mechanisms by which Mg ions promote osteogenic activity (Wu et al., 2015). In addition, given the rapid corrosion of Mg-based alloys that may hinder their clinical application, other authors have reported that surface coatings improve corrosion resistance while preserving both osteogenic potential and biocompatibility (Zhang et al., 2022).

The adhesion of osteoblasts to the biomaterial represents a fundamental step in validating its potential for bone regeneration, as proper anchorage is required to ensure subsequent proliferation, differentiation, and matrix mineralization. To assess this property, cell attachment both onto the biomaterial surface and in the surrounding area was verified, providing evidence of its cytocompatibility and suitability for

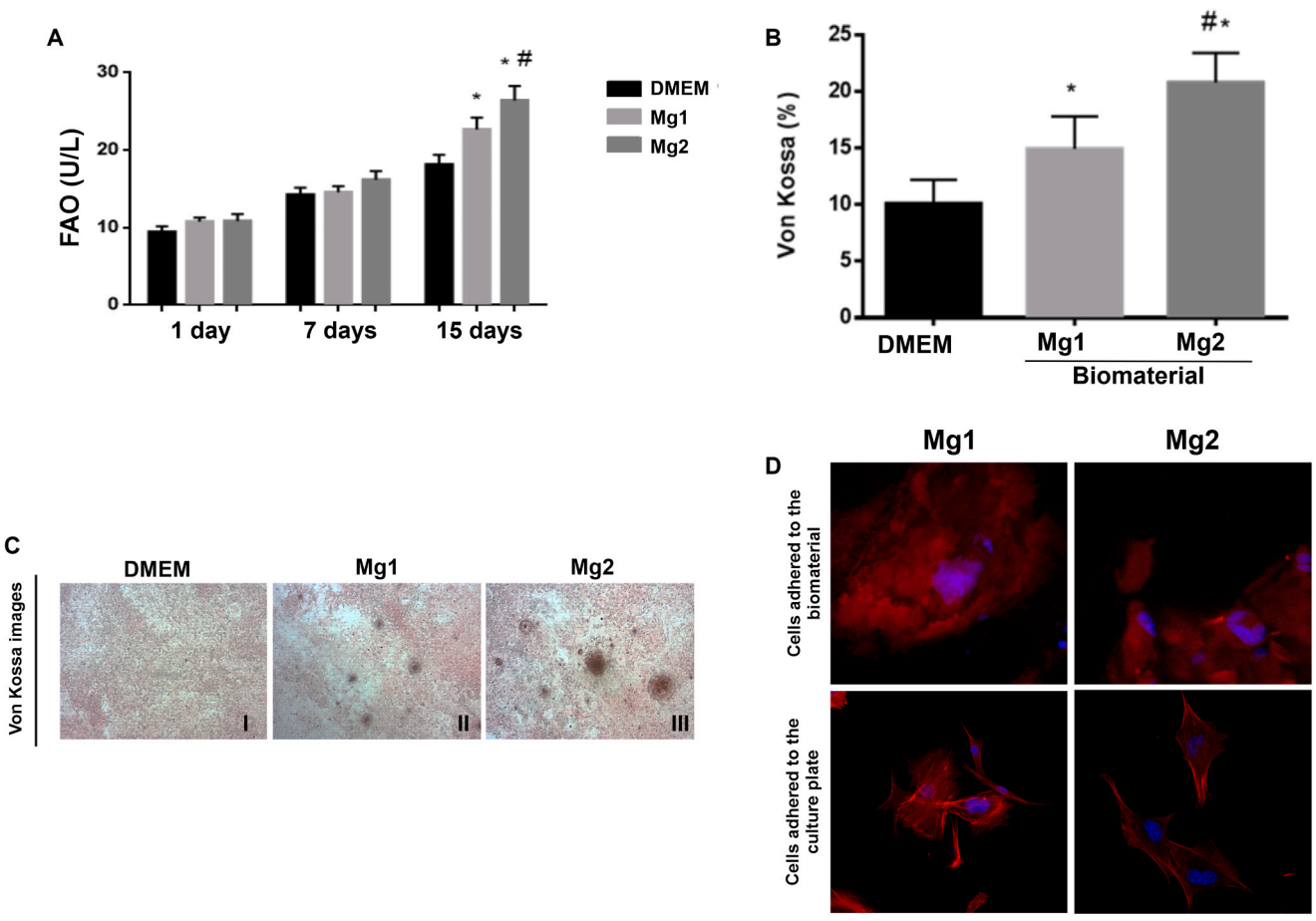

Fig. 3. A) Effect of Magnesium alloy without (Mg1) and with (Mg2) Calcium Phosphate coating on alkaline phosphatase levels (APL) produced by murine osteoblasts (OFCOL II) after 1, 7, and 15 days. DMEM group: cells cultured without biomaterial; Mg1 group: cells cultured with Mg1; Mg2 group: cells cultured with Mg2. B) Quantification of calcium deposits in the mineralization assay described by Von Kossa in OFCOL II osteoblasts after 21 days of culture. The result is expressed as a percentage of occupation by mineral nodules. *P < 0.05 compared to the DMEM group and #P < 0.05 compared to each other (Mg1 and Mg2). C) Representative images of the mineralization assay described by Von Kossa. CI) Presence of mineralization nodules in the DMEM group after 21 days of testing; CII) Presence of mineralization nodules in the Mg1 group after 21 days of testing; CIII) Presence of mineralization nodules in the Mg2 group after 21 days of testing. D) Representative images from the immunofluorescence assay.

osteogenic applications. Our data showed that the cells in the surroundings of the biomaterial exhibited a spread morphology, suggesting that they remained viable and metabolically active. In contrast, cells cultured directly on the biomaterial did not display the typical morphology of active osteoblasts, likely due to the irregular topography of the biomaterial, particularly in the Mg2 group. Similar observations were reported by Hiromoto and Yamazaki (2016), who investigated osteoblasts' behavior on calcium phosphate-coated materials and found that the larger spacing between crystal tips hindered the extension of cellular pseudopodia toward adjacent structures. This may account for the atypical morphology observed in cells cultured directly on the biomaterial in the Mg1 and Mg2 groups, despite their viability. In contrast, cells adhered in the surrounding area exhibited morphology and behavior comparable to those of cells grown exclusively in culture medium. This observation further supports the notion that the cells attached to the samples remained viable, considering that the culture medium within the well was also influenced by the biomaterial, even though the material did not occupy the entire surface area.

Apoptosis plays a fundamental role in maintaining tissue homeostasis by balancing cell proliferation and programmed cell death. This process is mediated by caspases, which are critical for the proper development and function of multicellular organisms (Bonyadi Rad et al., 2017). Among them, caspase-3 is considered a key executioner of apoptosis, typically present in cells in an inactive form that, upon apoptotic stimulation, is cleaved into its active form by initiator caspases (Ghavami et al., 2009). In the present study, apoptotic markers were employed to assess whether osteoblasts underwent apoptosis following contact with Mg-based alloys. The results demonstrated that both Mg1 and Mg2 groups exhibited a comparable reduction in caspases 3 and 9 levels, indicating preserved cell survival despite the altered morphology observed.

The RANK/RANKL/OPG signaling axis is a pivotal regulatory system in bone remodeling and repair. During the initial stages of bone healing, RANKL expression increases to stimulate osteoclast activity and promote the resorption of damaged tissue. Subsequently, OPG expression is upregulated to counteract RANKL, thereby suppressing osteoclastogenesis and favoring new bone formation (Ono et al., 2020). In parallel, bone morphogenetic proteins (BMPs), particularly BMP-2, play a central role in osteoblast differentiation and can also modulate osteoclast function both directly and indirectly through interactions with the RANK/RANKL/OPG pathway (Lademann et al., 2020). Based on this, the present study examined the involvement of the RANK/RANKL/OPG signaling cascade and BMP-2 in the activation of osteoblasts, aiming to elucidate the potential mechanism through which Mg alloys (Mg1 and Mg2) mediate osteogenic activity.

Our data showed a significant increase in OPG and BMP-2 expression in osteoblasts cultured with the Mg-based biomaterials compared to the control group, suggesting the involvement of the RANK/RANKL/OPG

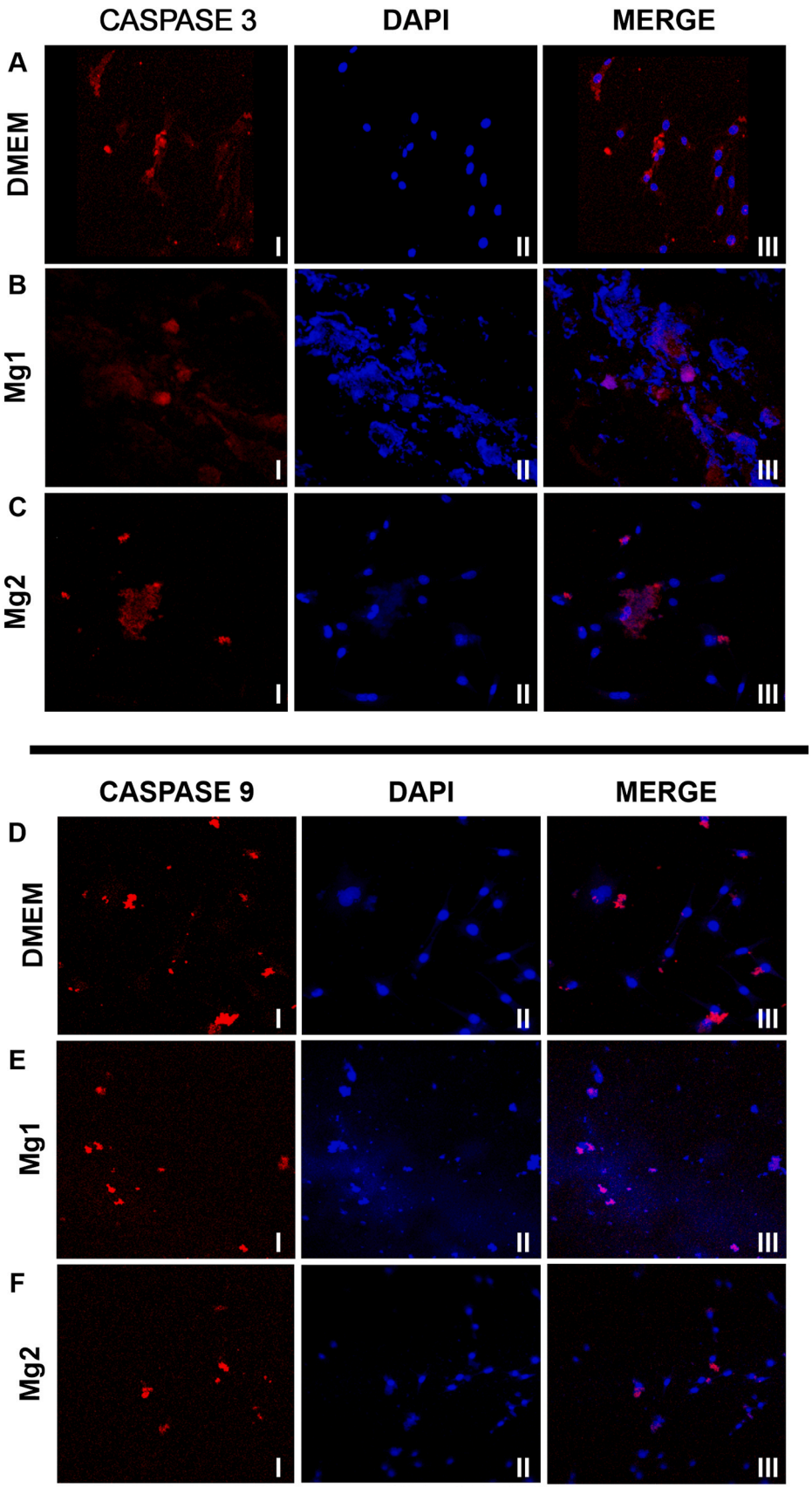

(caption on next page)

Fig. 4. Immunofluorescence images for caspase 3. AI, BI, and CI: immunostaining for caspase 3 (red) in the DMEM, Mg1, and Mg2 groups, respectively. AII, BII, and CII: cell nucleus immunostaining with DAPI (blue) in DMEM, Mg1, and Mg2 groups, respectively. AIII, BIII, and CIII: cytoplasmic immunostaining of caspase 3 (red) and DAPI (blue) in the DMEM, Mg1, and Mg2 groups, respectively. Immunofluorescence images for caspase 9. DI, EI, and FI: immunostaining for caspase 9 (red) in the DMEM, Mg1, and Mg2 groups, respectively. DII, EII, and FII: cell nucleus immunostaining with DAPI (blue) in DMEM, Mg1, and Mg2 groups, respectively. DIII, EIII, and FIII: cytoplasmic immunostaining of caspase 9 (red) and DAPI (blue) in the DMEM, Mg1, and Mg2 groups, respectively.

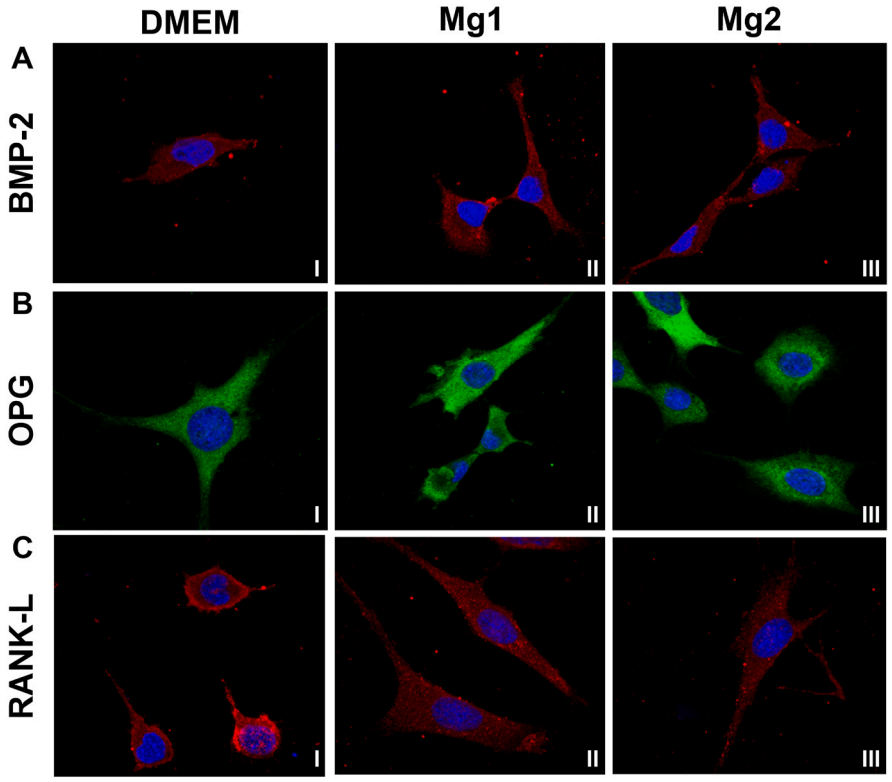

D

	DMEM	Mg1	Mg2
BMP-2	1 (1-2)	2 (2-3)*	2 (2-3)*
OPG	2 (1-3)	3 (2-3)*	3 (2-3)*
RANK-L	2 (1-3)	2 (1-3)	2 (1-3)

Fig. 5. Representative immunofluorescence images. AI, BI and CI: Expression of BMP-2, OPG and RANK-L proteins in the DMEM group, respectively; AII, BII and CII: Expression of BMP-2, OPG and RANK-L proteins in the Magnesium group (Mg1), respectively; AIII, BIII and CIII: Expression of BMP-2, OPG and RANK-L proteins in the Magnesium group coated with Calcium Phosphate (Mg2), respectively. The table shows the quantitative analysis of immunostaining intensity of BMP-2, OPG, and RANK-L expressed as median, minimum, and maximum values. All data were analyzed using the Kruskal-Wallis test followed by Dunn's multiple comparison test. *$P < 0.05$ vs DMEM group.

signaling pathway and BMP-2 upregulation in mediating the osteogenic potential of Mg alloys in murine osteoblast cells (OFCOLL II). Notably, Mg supplementation has been reported to increase OPG levels during bone repair, thereby favoring bone formation (Liu et al., 2024). In line with these observations, Tatullo et al. (2024) found a positive association between Mg coatings and BMP2 expression (Tatullo et al., 2024). Furthermore, complementary evidence from both in vitro and in vivo studies supports the osteogenic and angiogenic effects of Mg-based strategies: Liu et al. (2024) reported that an injectable gellan gum (GG)-based hydrogel incorporating nano-hydroxyapatite (nHA) and magnesium sulfate ($MgSO_4$) promoted osteogenesis and angiogenesis in bone defect repair (Liu et al., 2024). Collectively, these data reinforce the role of Mg in promoting bone regeneration through coordinated regulation of osteogenic signaling pathways.

5. Conclusions

In this study, we developed a magnesium alloy without (Mg1) and with (Mg2) a chemically deposited calcium phosphate (CaP) coating. Both alloys demonstrated osteogenic effects *in vitro,* with no evidence of cytotoxicity and no impairment of osteoblast proliferation. Furthermore, Mg1 and Mg2 groups exhibited a comparable reduction in

caspases 3 and 9 expression, indicating preserved cell viability despite morphological alterations. Importantly, Mg alloys also appear to modulate osteoblast function through the regulation of RANK/RANKL/OPG signaling and the stimulation of BMP-2. Within the limitations of the current investigation, our results provide evidence that Mg alloys with CaP coating may represent a promising alternative strategy for bone regeneration, offering potential translational applications in future clinical settings. However, further studies, including in vivo models and long-term evaluations, are required to validate and expand these findings.

CRediT authorship contribution statement

Matheus Brandão dos Santos Lopes: Methodology, Investigation, Formal analysis. **Rosemayre Souza Freire:** Visualization, Validation, Formal analysis. **Yves Ramos Costa Beviláqua:** Methodology, Investigation, Formal analysis. **Stephany Ellen de Castro:** Methodology, Investigation, Formal analysis. **Abrahão Cavalcante Gomes de Souza Carvalho:** Validation, Supervision. **Mariana de Oliveira Viana Veras:** Resources, Methodology, Investigation, Formal analysis. **Pierre Basílio Almeida Fechine:** Validation, Project administration. **Paula Goes:** Writing – original draft, Supervision, Project administration. **Fátima Regina Nunes de Sousa:** Writing – review & editing, Writing – original draft, Supervision, Formal analysis. **Gildênio Estevam Freire:** Methodology, Investigation, Formal analysis. **Thâmara Manoela Marinho Bezerra:** Supervision, Methodology, Investigation, Formal analysis. **Mirna Marques Bezerra:** Writing – review & editing, Writing – original draft, Formal analysis. **Ana Beatriz Graça Duarte:** Validation, Supervision. **Renata Ferreira Carvalho Leitão:** Writing – review & editing, Supervision, Project administration, Funding acquisition, Formal analysis, Data curation, Conceptualization. **Conceição Silva Martins:** Supervision, Methodology, Formal analysis, Data curation.

Funding

This work was supported by the Postgraduate Program in Morpho-functional Sciences (PCMF) at the Federal University of Ceará, in Brazil.

Declaration of Competing Interest

The authors declare that they have no known competing financial interests or personal relationships that could have appeared to influence the work reported in this paper.

Acknowledgements

We are grateful to the Nucleus of Study in Microscopy and Image Processing (NEMPI), Department of Morphology of Federal University of Ceará (UFC) for histology and digital imaging services; Central Analítica UFC (open facility funded by FINEP – CT - Infra, CAPES-Pró-Equipamentos, and MCTI-CNPq-SisNano2.0) for support with scanning electron microscopy SEM and to the Laboratory of Microscopy for technical assistance.

Data availability

Data will be made available on request.

References

Arganda-Carreras, I., Kaynig, V., Rueden, C., Schindelin, J., Cardona, A., Seung, H.S., 2017. Trainable Weka segmentation: a machine learning tool for microscopy pixel classification. Bioinformatics 33 (15), 2424–2426. https://doi.org/10.1093/bioinformatics/btx180.

Benoit, D.S., Schwartz, M.P., Durney, A.R., Anseth, K.S., 2008. Small functional groups for controlled differentiation of hydrogel-encapsulated human mesenchymal stem cells. Nat. Mater. 7 (10), 816–823. https://doi.org/10.1038/nmat2269.

Black, C.R., Goriainov, V., Gibbs, D., Kanczler, J., Tare, R.S., Oreffo, R.O., 2015. Bone tissue engineering. Curr. Mol. Biol. Rep. 1 (3), 132–140. https://doi.org/10.1007/s40610-015-0022-2.

Bonyadi Rad, E., Mostofi, S., Katschnig, M., Stanzl-Tschegg, S., Pippan, R., Zaffe, D., Reiter, C., Weinberg, A.M., 2017. Differential apoptotic response of MC3T3-E1 pre-osteoblasts to biodegradable magnesium alloys in an in vitro direct culture model. J. Mater. Sci. Mater. Med. 28 (10), 155. https://doi.org/10.1007/s10856-017-5969-5.

Cheng, M.Q., Wahafu, T., Jiang, G.F., Liu, W., Qiao, Y.Q., Peng, X.C., Cheng, T., Zhang, X.L., He, G., Liu, X.Y., 2016. A novel open-porous magnesium scaffold with controllable microstructures and properties for bone regeneration. Sci. Rep. 6 (1), 24134. https://doi.org/10.1038/srep24134.

Cherkaev, E., Bonifasi-Lista, C., 2011. Characterization of structure and properties of bone by spectral measure method. J. Biomech. 44 (2), 345–351. https://doi.org/10.1016/j.jbiomech.2010.10.031.

Cowin, S.C., 2001. Informa Healthcare, New York. Bone Mechanics Handbook, second. https://doi.org/10.1201/b14263.

Cui, F.Z., Yang, J.X., Jiao, Y.P., Yin, Q.S., Zhang, Y., Lee, I.S., 2008. Calcium phosphate coating on magnesium alloy for modification of degradation behavior. Front. Mater. Sci. China 2 (2), 143–148. https://doi.org/10.1007/s11706-008-0024-6.

Farag, M.M., 2023. Recent trends on biomaterials for tissue regeneration applications: review. J. Mater. Sci. 58, 527–558. https://doi.org/10.1007/s10853-022-08102-x.

Fedchenko, N., Reifenrath, J., 2014. Different approaches for interpretation and reporting of immunohistochemistry analysis results in the bone tissue – a review. Diagn. Pathol. 9, 221. https://doi.org/10.1186/s13000-014-0221-9.

Ghavami, S., Hashemi, M., Ande, S.R., Yeganeh, B., Xiao, W., Eshraghi, M., Bus, C.J., Kadkhoda, K., Wiechec, E., Halayko, A.J., Los, M., 2009. Apoptosis and cancer: mutations within caspase genes. J. Med. Genet 46 (8), 497–510. https://doi.org/10.1136/jmg.2009.066944.

Gonzalez, J., Hou, R.Q., Nidadavolu, E.P., Willumeit-Römer, R., Feyerabend, F., 2018. Magnesium degradation under physiological conditions – best practice. Bioact. Mater. 3 (2), 174–185. https://doi.org/10.1016/j.bioactmat.2018.01.003.

Hart, N.H., Nimphius, S., Rantalainen, T., Ireland, A., Siafarikas, A., Newton, R.U., 2017. Mechanical basis of bone strength: influence of bone material, bone structure and muscle action. J. Musculoskelet. Neuron Inter. 17 (3), 114–139.

Hiromoto, S., Yamazaki, T., 2017. Micromorphological effect of calcium phosphate coating on compatibility of magnesium alloy with osteoblast. Sci. Technol. Adv. Mater. 18 (1), 96–109. https://doi.org/10.1080/14686996.2016.1266238.

Iskandar, M.E., Aslani, A., Tian, Q., Liu, H., 2015. Nanostructured calcium phosphate coatings on magnesium alloys: characterization and cytocompatibility with mesenchymal stem cells. J. Mater. Sci. Mater. Med. 26 (5), 224. https://doi.org/10.1007/s10856-015-5512-5.

Jilka, R.L., Noble, B., Weinstein, R.S., 2013. Osteocyte apoptosis. Bone 54 (2), 264–271. https://doi.org/10.1016/j.bone.2012.11.038.

Kieke, M., Feyerabend, F., Lemaitre, J., Behrens, P., Willumeit-Römer, R., 2016. Degradation rates and products of pure magnesium exposed to different aqueous media under physiological conditions. BioNanoMaterials 17 (3–4), 163–174. https://doi.org/10.1515/bnm-2015-0020.

Klammert, U., Reuther, T., Jahn, C., Kraski, B., Kübler, A.C., Gbureck, U., 2009. Cytocompatibility of brushite and monetite cell culture scaffolds made by three-dimensional powder printing. Acta Biomater. 5 (2), 727–734. https://doi.org/10.1016/j.actbio.2008.08.019.

Köhler, C., Orrenius, S., Zhivotovsky, B., 2002. Evaluation of caspase activity in apoptotic cells. J. Immunol. Methods 265 (1–2), 97–110. https://doi.org/10.1016/S0022-1759(02)00073-X.

Lademann, F., Hofbauer, L.C., Rauner, M., 2020. The bone morphogenetic protein pathway: the osteoclastic perspective. Front. Cell Dev. Biol. 8, 586031. https://doi.org/10.3389/fcell.2020.586031.

Liu, H., Li, K., Guo, B., Yuan, Y., Ruan, Z., Long, H., Zhu, J., Zhu, Y., Chen, C., 2024. Engineering an injectable gellan gum-based hydrogel with osteogenesis and angiogenesis for bone regeneration. Tissue Cell 86, 102279. https://doi.org/10.1016/j.tice.2023.102279.

Liu, L., Luo, P., Wen, P., Xu, P., 2024. The role of magnesium in the pathogenesis of osteoporosis. Front. Endocrinol. (Lausanne) 15, 1406248. https://doi.org/10.3389/fendo.2024.1406248.

Marco, I., Myrissa, A., Martinelli, E., Kuehn, S., Feyerabend, F., Willumeit-Römer, R., 2017. In vivo and in vitro degradation comparison of pure Mg, Mg-10Gd and Mg-2Ag: a short-term study. Eur. Cell Mater. 33, 90–104. https://doi.org/10.22203/eCM.v033a07.

Moss, D.W., 1982. Alkaline phosphatase isoenzymes. Clin. Chem. 28 (10), 2007–2016.

Nogueira-Júnior, V., Sousa, F.R.N., Rebouças, C.S.M., Veras, D.S., Moraes, M.O., Brayner, M.M.B., et al., 2024. Exploring the osteogenic potential of semisynthetic triterpenes from Combretum leprosum: an in vitro and in silico study. Vitr. Cell Dev. Biol. Anim. 60 (8), 853–867. https://doi.org/10.1007/s11626-024-00928-w.

Ono, T., Hayashi, M., Sasaki, F., Nakashima, T., 2020. RANKL biology: bone metabolism, the immune system, and beyond. Inflamm. Regen. 40, 2. https://doi.org/10.1186/s41232-019-0111-3.

Oriňaková, R., Gorejová, R., Orságová Králová, Z., Oriňak, A., 2020. Surface modifications of biodegradable metallic foams for medical applications. Coatings 10 (9), 819. https://doi.org/10.3390/coatings10090819.

Park, K.D., Lee, B.A., Piao, X.H., Kim, H.S., Lee, Y.M., 2013. Effect of magnesium and calcium phosphate coatings on osteoblastic responses to the titanium surface. J. Adv. Prosthodont 5 (4), 402–408. https://doi.org/10.4047/jap.2013.5.4.402.

Pereira, A., Vaz, P., Rocha, G., Felino, A., Tavares, P., 2011. Engenharia genética em implantologia – o RANKL. Rev. Port. Estomatol. Med. Dent. Cir. Maxilofac. 52 (3), 170–174. https://doi.org/10.1016/j.rpemd.2011.06.001.

Pires, A.L., Bierhalz, A.C., Moraes, Â.M., 2015. Biomaterials: types, applications, and market. Quim. Nova. https://doi.org/10.5935/0100-4042.20150094.

Saleh, M.M., Touny, A.H., Al-Omair, M.A., Saleh, M.M., 2016. Biodegradable/biocompatible coated metal implants for orthopedic applications. Biomed. Mater. Eng. 27 (1), 87–99. https://doi.org/10.3233/bme-161568.

Sezer, N., Evis, Z., Kayhan, S.M., Tahmasebifar, A., Koç, M., 2018. Review of magnesium-based biomaterials and their applications. J. Magnes. Alloy. 6 (1), 23–43. https://doi.org/10.1016/j.jma.2018.02.003.

Song, Y., Zhang, S., Li, J., Zhao, C., Zhang, X., 2010. Electrodeposition of Ca–P coatings on biodegradable Mg alloy: in vitro biomineralization behavior. Acta Biomater. 6 (5), 1736–1742. https://doi.org/10.1016/j.actbio.2009.12.020.

Tatullo, M., Piattelli, A., Ruggiero, R., Santacroce, L., Cocco, A., Codispoti, B., et al., 2024. Functionalized magnesium alloys obtained by superplastic forming process retain osteoinductive and antibacterial properties: an in vitro study. Dent. Mater. 40 (3), 557–562. https://doi.org/10.1016/j.dental.2024.01.005.

Wang, Y., 2011. Sol–gel derived hydroxyapatite coatings on metallic implants: characterization, in vitro and in vivo analysis. In: Zhang, S. (Ed.), Biological and Biomedical Coatings Handbook. CRC Press, Boca Raton, pp. 16–59. https://doi.org/10.1201/b10871-6.

Wennberg, C., Hessle, L., Lundberg, P., Kozlova, I., Wendel, M., Anderson, H.C., Marks Jr., S.C., Millán, J.L., Andersson, G., 2000. Functional characterization of osteoblasts and osteoclasts from alkaline phosphatase knockout mice. J. Bone Miner. Res. 15 (10), 1879–1888. https://doi.org/10.1359/jbmr.2000.15.10.1879.

Wong, H.M., Zhao, Y., Tam, V., Wu, S., Chu, P.K., Zheng, Y., To, M.K.T., 2013. In vivo stimulation of bone formation by aluminum and oxygen plasma surface-modified magnesium implants. Biomaterials 34 (38), 9863–9876. https://doi.org/10.1016/j.biomaterials.2013.08.052.

Wu, L., Feyerabend, F., Schilling, A.F., Willumeit-Römer, R., Luthringer, B.J.C., 2015. Effects of extracellular magnesium extract on the proliferation and differentiation of human osteoblasts and osteoclasts in coculture. Acta Biomater. 27, 294–304. https://doi.org/10.1016/j.actbio.2015.08.042.

Xie, J., Riley, C., Kumar, M., Chittur, K., 2002. FTIR/ATR study of protein adsorption and brushite transformation to hydroxyapatite. Biomaterials 23 (17), 3609–3616. https://doi.org/10.1016/S0142-9612(02)00090-X.

Xin, Y., Huo, K., Tao, H., Tang, G., Chu, P.K., 2008. Influence of aggressive ions on the degradation behavior of biomedical magnesium alloy in physiological environment. Acta Biomater. 4 (6), 2008–2015. https://doi.org/10.1016/j.actbio.2008.05.014.

Zhang, K., Wang, S., Zhou, C., Cheng, L., Gao, X., Xie, X., et al., 2018. Advanced smart biomaterials and constructs for hard tissue engineering and regeneration. Bone Res 6, 31. https://doi.org/10.1038/s41413-018-0032-9.

Zhang, Z., Sun, X., Yang, J., Wang, C., 2022. In vitro evaluation of freeze-drying chitosan–mineralized collagen/Mg–Ca alloy composites for osteogenesis. J. Biomater. Appl. 36 (8), 1359–1377. https://doi.org/10.1177/08853282211049296.